A highly stable and fully tunable open microcavity platform at cryogenic temperatures

Maximilian Pallmann, Timon Eichhorn, Julia Benedikter, et al.

View Online   Export Citation   CrossMark

ARTICLES YOU MAY BE INTERESTED IN
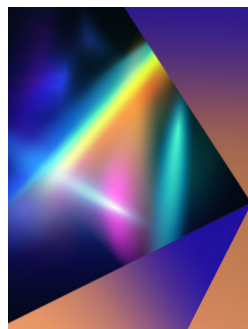
APL Photonics

Applications Now Open for the
Early Career Editorial Advisory Board

Learn more and submit!

AIP Publishing

A highly stable and fully tunable open microcavity platform at cryogenic temperatures

View Online   Export Citation   CrossMark

Maximilian Pallmann,[1] [ID] Timon Eichhorn,[1] [ID] Julia Benedikter,[2] Bernardo Casabone,[3] [ID] Thomas Hümmer,[2,4] and David Hunger[1,5a)] [ID]

AFFILIATIONS

[1] Physikalisches Institut, Karlsruhe Institute of Technology (KIT), Wolfgang-Gaede Str. 1, 76131 Karlsruhe, Germany
[2] Faculty of Physics, Ludwig-Maximilians-University (LMU), Schellingstr. 4, 80799 Munich, Germany
[3] ICFO-Institut de Ciencies Fotoniques, The Barcelona Institute of Science and Technology, 08860 Castelldefels, Barcelona, Spain
[4] Qlibri GmbH, Maistr. 67, 80337 Munich, Germany
[5] Institute for Quantum Materials and Technologies (IQMT), Karlsruhe Institute of Technology (KIT), Herrmann-von-Helmholtz Platz 1, 76344 Eggenstein-Leopoldshafen, Germany

[a)] Author to whom correspondence should be addressed: david.hunger@kit.edu

ABSTRACT

Open-access microcavities are a powerful tool to enhance light–matter interactions for solid-state quantum and nanosystems and are key to advance applications in quantum technologies. For this purpose, the cavities should simultaneously meet two conflicting requirements—full tunability to cope with spatial and spectral inhomogeneities of a material and highest stability under operation in a cryogenic environment to maintain resonance conditions. To tackle this challenge, we have developed a fully tunable, open-access, fiber-based Fabry–Pérot microcavity platform that can be operated under increased noise levels in a closed-cycle cryostat. It comprises custom-designed monolithic micro- and nanopositioning elements with up to mm-scale travel range that achieve a passive cavity length stability at low temperature of only 15 pm rms in a closed-cycle cryostat and 5 pm in a more quiet flow cryostat. This can be further improved by active stabilization, and even higher stability is obtained under direct mechanical contact between the cavity mirrors, yielding 0.8 pm rms during the quiet phase of the closed-cycle cryocooler. The platform provides the operation of cryogenic cavities with high finesse and small mode volume for strong enhancement of light–matter interactions, opening up novel possibilities for experiments with a great variety of quantum and nanomaterials.

I. INTRODUCTION

Open-access optical microcavities are a versatile platform to enable the enhancement of light–matter interactions for quantum and nanosystems with a broad range of applications such as efficient single photon sources[1–7] and spin-photon interfaces,[8–10] single emitter strong coupling,[11,12] exciton polaritons,[13–16] and cavity optomechanics.[17–19] In order to achieve good coherence properties, most of the materials have to be cooled down to cryogenic temperatures. For the example of solid state quantum emitters, stringent requirements on the coherence, particular transition frequency, local spin environment, etc., typically require a careful selection of suitable emitters from a large set of candidates. A cavity platform integrated in a cryostat that is capable of finding *in situ* suitable emitters on such spatially inhomogeneous samples and addressing optical transitions across a large spectral range is thus highly desirable.

Using a closed-cycle cryostat provides advantages in terms of usability as well as scalability but poses a challenge due to the increased mechanical noise level compared to wet cryostats. Although current commercial solutions offer mechanical vibrations of the experimental cold plate down to a few nm root mean square (rms), this still remains a severe challenge for operating a high-finesse microcavity. For example, maintaining resonance conditions for a cavity with a finesse of $F = 20\,000$ at a wavelength of 580 nm requires a cavity length stability of less than the spatial linewidth $\Delta L = \lambda/2F = 15$ pm, i.e., three orders of magnitude lower than the vibrations of the cold plate. The figure of merit for the light–matter

interaction between cavity photons and the quantum emitter is the Purcell factor $C \propto F/w_0^2$ with w_0 the cavity mode waist at the emitter. Assuming a Gaussian broadening of the cavity linewidth due to mechanical vibrations, the time-averaged Purcell factor of system C is decreased with respect to the resonant Purcell factor C_0 according to[20]

$$\frac{C(\Delta L, \sigma)}{C_0} = \sqrt{\frac{\pi}{8}} \frac{\Delta L}{\sigma} e^{\frac{\Delta L^2}{8\sigma^2}} \left(1 - \mathrm{erf}\left(\frac{\Delta L}{2\sqrt{2}\sigma}\right)\right), \tag{1}$$

where σ denotes the rms cavity length jitter. This effective Purcell factor is plotted in Fig. 1 for a cavity finesse of 20 000 and 100 000, respectively, normalized to the latter. From this, one can see that a length stability corresponding to one cavity linewidth ΔL leads to a reduction of 40% of the resonant Purcell factor. The aim is therefore to minimize the length jitter to the level of a few pm.

In the past years, significant progress has been made to reach such high mechanical stability by using passive vibration isolation techniques as well as active feedback.[10,11,20–24] However, for platforms operated in closed-cycle cryostats, the best stability reached so far is about 14 pm rms during the quiet phase of the cryostat cycle using active stabilization.[20]

In this work, we present two variants of custom-designed, fully tunable open-access Fabry–Pérot microcavities that are designed for the operation in a flow cryostat and a closed-cycle cryostat, respectively. At room temperature and when the cryostat is switched off, we reach a stability of 1 pm rms under active stabilization. At cryogenic temperatures and operated in the flow (closed-cycle) cryostat, we achieve a passive stability of 5(15) pm rms. This makes it possible to perform experiments without the need for active stabilization, which typically requires a separate locking laser at a different wavelength that limits the useable cavity lengths. Active stabilization can further improve this, and we achieve a stability of 2.5(15) pm rms in the flow (closed-cycle) cryostat. Operating the cavity in a contact mode by bringing the fiber mirror into mechanical contact with the planar opponent, we achieve a stability of 0.7 pm rms in the flow
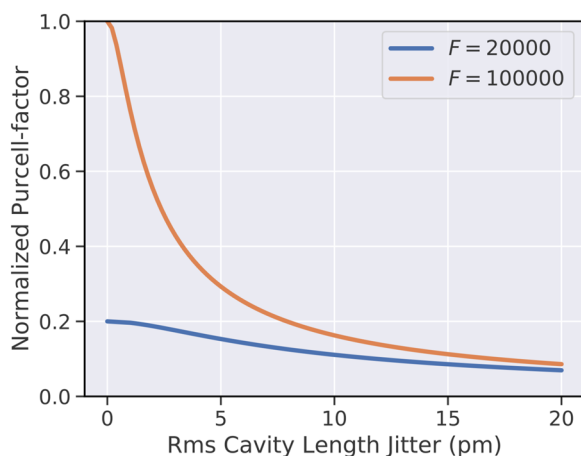
cryostat and 0.8 pm rms during the quiet phase of the closed-cycle cryostat cycle.

II. EXPERIMENTAL METHODS

Our cavity platform is a home-built design based on a custom-developed nanopositioning platform. The design relies on piezo actuator stacks and electrical DC motors to achieve full tunability of the fiber-based Fabry–Pérot cavity down to cryogenic temperatures. As shown schematically in Fig. 2(a), the cavity consists of a macroscopic planar distributed Bragg reflector (DBR) mirror, which typically carries the sample that shall be investigated. The second mirror consists of a single-mode optical fiber where a concave depression has been machined onto the end facet by CO_2-laser machining,[25] which is then again coated with a DBR. The laser light enters the cavity via the fiber. We use single mode optical fibers, which are not polarization maintaining. With a $\lambda/4$ and a $\lambda/2$ wave plate before the fiber coupling, we can pre-compensate for the arbitrary polarization rotation of the fiber to prepare a defined linear polarization of the probe light at the cavity. We do not observe degradation of cavity properties upon cooldown. As the setups presented in this work are designed for the investigation of different samples, we run the experiments with different coatings and laser wavelengths, and thereby also with different design finesses. This influences the required stability and performance of an active feedback system, since a higher finesse resonance enables more precise feedback while having the drawback of a smaller stabilization range.

A. Design of the cavity platform

To achieve the highest passive mechanical stability, we have designed a monolithic cavity nanopositioning stage [Figs. 2(a), 2(b), and 2(c)] based on flexure-mechanical elements and piezo actuators for fine tuning that can cover an (x, y, z)-volume of $(70 \times 70 \times 10)$ μm^3 at room temperature that reduces to $\sim (10 \times 10 \times 1.5)$ μm^3 at 10 K [Fig. 2(d)]. We calibrate the lateral scanning range by cavity transmission images of a planar mirror where a grid pattern with a pitch of 10 μm has been machined by CO_2-laser shots. During the cooldown, repeated scanning cavity images reveal a shift of the fiber position to the right due to differential thermal contraction of the piezo actuators and the frame. In addition, the scanning range decreases due to the capacity reduction of the piezo stacks. For coarse tuning over a volume of $(2 \times 2 \times 2)$ mm³, the stage incorporates electromotors and gear work. The central mechanical element is a flexural lever arm to which the cavity fiber is fixed, which itself is glued into a steel needle to increase mechanical stability. The assembly is preloaded by three piezo-electric actuators that allow bending motions to achieve three-dimensional nanopositioning of the fiber tip. There are screws to control the prestress on the x- and y-piezo actuators, which are also used to bend the fiber needle and thus allow for angular alignment of the fiber tip. The lever arm design aims for low weight and small dimensions in combination with a high stiffness. This ensures high mechanical resonance frequencies of several kHz in order to avoid coupling to acoustic noise. Furthermore, the noise sources are reduced by clamping the fiber and all cables connected to the top frame. The positioning along the cavity axis (z) requires particular attention, since it should simultaneously allow one to tune across several longitudinal cavity resonances, i.e.,

FIG. 1. Dependence of the averaged Purcell factor for a cavity of 20 000 finesse (blue) and 100 000 (orange) on the rms cavity length jitter. Both curves are normalized to the maximum Purcell factor for $F = 100 000$.
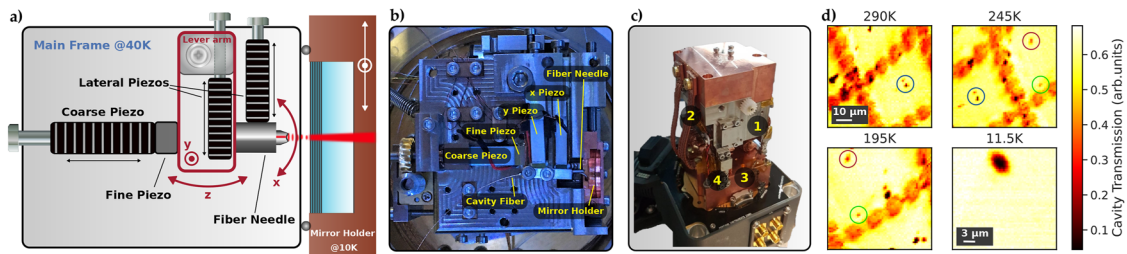
FIG. 2. (a) Schematic drawing of the cavity setup: the planar DBR-mirror (blue) and the fiber mirror can be moved laterally to select a region of interest on the sample. The mirror separation is controlled by two combined piezo stacks, referred to as coarse and fine piezo, that push the lever holding the fiber, which can be clamped onto the top frame to improve rigidness. (b) Top view photograph of the main frame, showing the central building blocks as shown in (a). (c) Photograph of the closed-cycle version of the cavity stage. 1: Top frame. 2: Thermal links. 3: Vibration isolation spring between the top and base frames. 4: Base frame. (d) Cavity transmission scans of a marker grid during a cooldown of the closed-cycle cryostat, showcasing the lateral drift of the fiber to the downright and the non-linear decrease in scanning range. The colored circles mark specific scatterers that can be tracked during the cooldown. When reaching the final temperature, the fiber position has left the grid, but a scattering particle on the planar mirror reveals the cavity point spread function.

a positioning range of a few micrometers, and to controllably maintain resonance conditions with sub-picometer resolution. The required overall dynamic range of 10^7 goes beyond the capability of available voltage sources to drive a single piezo. We thus physically separate the ultra-fine tuning with a thin piezo plate with ~100 nm expansion range (fine piezo) from the fine tuning with a piezo stack with a few micrometer tuning range (coarse piezo) under cryogenic conditions. Both piezos are separately driven by suitably filtered voltage sources and amplifiers. To obtain an even wider range of cavity length tunability over a few millimeters, a DC motor, which was slightly modified to work under cryogenic conditions, is used to move the piezo actuators in the longitudinal direction. We clean the motors and gear works from grease in warm soap water and acetone, shorten the motor axis, and increase the bearing diameter to avoid the motors getting stuck at low temperatures. The wide tuning range is necessary to compensate for thermal contraction upon the cooldown of the platform. We minimize the effects of thermal contraction by using titanium for the main frame as well as the lever arm, which has a low thermal expansion coefficient (8.6×10^{-6} K^{-1}). The planar mirror is mounted inside a copper mirror holder, which is thermally isolated from the main frame by glass spheres. It is pressed against the main frame by a spring to ensure mechanical stiffness while keeping the flexibility to move the mirror laterally with two additional DC motors over several millimeters.

B. Active stabilization

We investigated various active stabilization schemes, including Pound–Drever–Hall stabilization based on phase modulation as well as side of fringe locking [see Fig. 3(a)]. While the former is insensitive to laser intensity noise and has a larger capture range, it requires high-frequency modulation and a strongly amplified high-bandwidth detector (1–5 GHz). In addition, it suffers from parasitic Fabry–Perot resonances in the beam path.[26] Due to the much lower hardware requirements and the presence of other limiting factors for the lock performance, we thus predominantly use side of fringe stabilization. Therefore, we tune the cavity to the slope of a resonance, typically below half of the peak transmission, and generate an error signal with an avalanche photodiode (APD) from the transmitted

signal after the plane mirror. For small excursions from the set point, the cavity transmission changes approximately linearly with the cavity length, such that we can both monitor cavity length fluctuations as well as use the signal for active stabilization. The transmission signal of a Lorentzian cavity resonance when tuning the mirror separation is shown in Fig. 3(b), together with an exemplary time trace of the transmission when actively stabilized to the same resonance while the closed-cycle cryostat is running.

The main sources of instability are acoustic and mechanical vibrations and electrical noise—with frequencies ranging from tens of Hz up to tens of kHz—as well as slow drifts, mostly originating from the thermal expansion that can have time scales of several hours. We, therefore, run a combined lock containing two proportional–integral–derivative (PID) controllers (*Red Pitaya STEMlab* 125-14) based on field-programmable gate arrays (FPGAs), in the following, referred to as fast and slow PID, that can change the cavity length independently through the two piezo actuators controlling the cavity length. In the case of the closed-cycle system, the slow PID is software-based and runs on a multifunction I/O device (*National Instruments, PCIe*-6353). For the fast PID, we
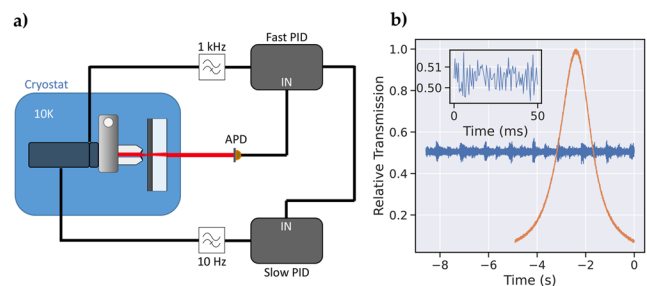
FIG. 3. (a) Simplified locking scheme used in this work. The fast PID is realized using a FPGA, while the slow lock is software-based in the closed-cycle system. (b) A representative cavity mode with its Lorentzian shape when sweeping the cavity length (horizontal axis in arbitrary units), together with a time trace of the same cavity mode when actively stabilized on the side of the fringe. The inset shows the time trace during the quiet phase of several hundred milliseconds between the strokes of the cold head piston of the closed-cycle cryostat.

use the cavity transmission signal measured by the APD as a reference signal to suppress the main contributions of noise. The PID output is fed to the locking piezo through a 1 kHz low-pass filter. As thermal drifts in the setup occur at a much slower time scale but with a larger amplitude, they are counteracted by the slow PID, which works similarly to the fast PID but uses the fast PID output as an error signal and is heavily low-pass filtered at 10 Hz.

C. Operation in a flow cryostat

One of our fiber cavity platforms is operated inside a customized KONTI microflow cryostat (CryoVac) and can be cooled down to 3.6 K. The cryostat has optical access via two windows such that light can be coupled out of the cavity via the planar mirror. Here, no vibration isolation is incorporated, and the cavity platform is placed on posts that are rigidly mounted onto the cryostat cold plate of a helium exchange gas chamber. Cooling via an exchange gas has the advantage of good thermalization of the sample under investigation and does not require thermal anchoring of the cavity stage to the cold plate. However, it leads to reduced piezo scan ranges since the elongation and force of the piezo stacks reduce with temperature. At the minimum temperature, we reach a longitudinal scan range of about 2 μm, i.e., six free spectral ranges, and lateral scanning over an area of 5×5 μm^2. To maintain the full tunability of the cavity, we use DC motors for the coarse tuning range of the cavity z-axis and lateral mirror movement.

To reduce acoustic noise, we are clamping all cables and pipes connected to the cryostat chamber. The main noise contribution in this system then comes from vibrations of the cold plate caused by the liquid helium flow through the heat exchanger beneath the cold plate. By adjusting the impedance of the helium return pipe via a proportional valve, we can reduce the vibrations of the cold plate and thus reach a quiet regime to operate the cavity.

D. Operation in a closed-cycle cryostat

The operation of a closed-cycle cryostat (Montana Cryostation CS1) makes it necessary to implement some adaptations. The vibrations introduced by the cryostat are significantly stronger compared to most flow or bath cryostats and range from frequencies below 100 Hz from the compressor itself up to several 10 kHz, being composed of electronic and mechanical noise.

The high frequency noise is expected to be more problematic than the lower frequencies, since it cannot be easily compensated easily via active stabilization. Therefore, the cavity platform is mechanically decoupled from the cold plate using steel springs with a loaded resonance frequency of a few ten of hertz that suppress the transmission of high-frequency noise to the cavity. Care was taken to use thin and rigidly fixed wiring of the elements on the cavity platform, typically using 0.2 mm thin phosphor bronze wires, to avoid mechanical short circuits.

In order to effectively cool down the titanium body of the main frame—considering the low thermal conductivity of titanium (22 W/mK)—we thermalize it to the radiation shield of the cryostat using super flexible copper braid stripes (*Copper Braid, SuperFlex* 0.2 mm). The flexibility of the braid is crucial, as one wants to avoid the transmission of vibrations that would counteract the effect of the springs. The braid, at the same time, acts as the damping system for the springs.

In the end, the only part of the cavity that needs to be cooled down to the lowest temperature is the sample, which is usually deposited on the macroscopic planar mirror, while all the other parts of the cavity platform can remain at a higher temperature. We, therefore, use a mirror holder made of copper that is thermally isolated from the main frame by a thermal spacer with minimal contact area. Moreover, a radiation shield made of copper encloses the stage. A thermalization link made from a braided mesh of high-conductivity copper filaments connecting the cold plate to the mirror holder was carefully optimized to achieve a minimal temperature gradient and the lowest vibration transmission. The resulting temperature is 10 K on the mirror holder, while the base block and the thermal shields show temperatures around 40 K, depending on the thermal load from laser radiation or the applied current for the motors.

III. RESULTS

For both devices presented here, we measure the mechanical transfer function of the cavity platform to characterize the mechanical resonances that are relevant for the stability of the system. We, therefore, apply a small sinusoidal voltage to the fine piezo while maintaining the cavity length stable with the drift compensation using the coarse piezo. We then measure the transmitted light intensity behind the planar mirror using an APD. The modulation frequency is swept from 100 Hz to 100 kHz with a logarithmic scale. The APD signal is fed into a lock-in amplifier, where it is mixed with the local oscillator and low-pass filtered to extract the phase and amplitude response of the system. Since the piezo excitation creates oscillations that will disperse across the cavity platform, the resulting transfer function reflects the reaction of the system to mechanical noise in the longitudinal direction, while it does not reveal how strongly vibrations from the cryostat couple to the cavity platform. We further quantify the mechanical stability of the cavity platform in two ways. First, we apply a drift compensation to the coarse piezo with a bandwidth of a few hertz, referred to as passive stability in the following. This drift compensation is used to keep the cavity at the slope of the resonance during the measurement time of several seconds. At base temperature, we observe hardly any thermal drifts, but piezo creep still leads to considerable drifts, which we have to compensate for. Second, this setting is compared to the stability under active stabilization with 1 kHz bandwidth, involving the fine piezo for fast feedback and the coarse piezo for drift compensation. For both techniques we record a time trace of the transmitted intensity through the cavity and investigate its fast Fourier transform (FFT, 100× averaged), yielding a power spectral density (PSD) that we convert into an amplitude spectral density of the cavity length fluctuations by using the first derivative of the Lorentzian cavity resonance at the locking setpoint.

A. Cavity stability in a flow cryostat

Running the flow cryostat at a temperature of 10 K in its quiet mode, as described earlier, we now investigate the mechanical stability of the cavity platform. The transfer function of the system, shown in Fig. 4(a), reveals that the first mechanical resonance occurs at around 4.5 kHz, and in the frequency band up to 50 kHz, plenty of resonances appear. Achieving such high frequencies of mechanical resonances was a central design principle, since this makes the
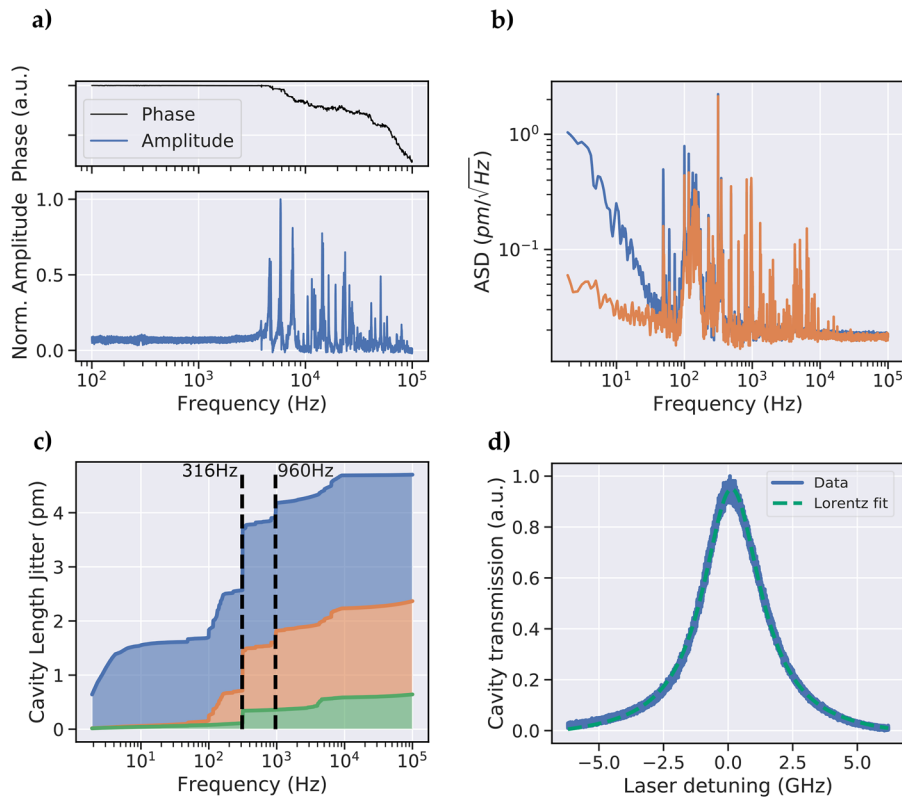
FIG. 4. Cavity stability at 10 K in the flow cryostat. (a) Magnitude and phase of the cavity transfer function. (b) Amplitude spectral density of an actively stabilized cavity transmission signal (orange) vs a passively stable cavity (blue). (c) Cumulative cavity length noise obtained from the ASD for the passive cavity (blue), actively stabilized open cavity (orange), and with the fiber in mechanical contact (green). (d) Cavity spectroscopy of the high finesse resonance at 580 nm in contact mode corresponding to the 11th mode order.

system inert against the dominant acoustic noise and enables a high bandwidth for active stabilization.

With these findings, we investigated active stabilization and optimized the electrical setup and PID controller settings to achieve a minimal rms value for an actively stabilized cavity. The amplified slow PID output for the drift compensation, which is applied to the coarse piezo, has to be low-pass filtered at a few hertz to avoid 50 Hz noise stemming from the amplifier. We manually optimize the parameters of the fast PID while monitoring the locked cavity length jitter. We find a unity-gain frequency and digital low-pass filtering at 800 Hz to give the best value of $\Delta z \approx 2.5$ pm rms. The comparison of the amplitude spectral density (ASD) of the passive (blue) and active (orange) cavity length jitter in Fig. 4(b) reveals a strong effect of the lock for frequencies below 100 Hz. For frequencies above 10 kHz, we are limited by the noise floor of the measurement electronics and laser noise. To calculate the cumulative rms values in Fig. 4(c), we subtracted an independently measured background spectrum for frequencies above 9 kHz since there is no apparent noise contribution from the cavity. The cumulative rms values show that the amplitude of the mechanical resonances around 150 and 316 Hz is also reduced by the active feedback. This can be seen by the reduced jumps in the orange curve compared to the blue one. Note that the cumulative rms values add up nonlinearly. Hence, the same step height at a high base level in the blue curve actually corresponds to a larger increase in the rms value than for the orange curve at a lower base level. We attribute these resonances and the one at 960 Hz to the structural response function of the entire cavity platform and

cryostat since they do not appear in the transfer function. The step at 6 kHz in the cumulative noise may be attributed to the strongest resonance of the lever arm, which can also be seen in the transfer function in Fig. 4(a).

When studying the cavity without active feedback, we find that the passive stability of the setup is very high, reaching a value of $\Delta z \approx 5$ pm rms. Passive stability can be improved by up to an order of magnitude when controllably bringing the fiber into mechanical contact with the planar mirror. Mechanical contact can be monitored by modulating the cavity length and observing the separation of two adjacent cavity resonances when approaching the two mirrors by increasing an offset voltage. As soon as contact is established, the resonances increase their separation. Besides that, no major impact on the cavity performance was observed. In some specific cases, however, it could be possible that the mode matching between the fiber and cavity modes decreases due to a slight angular misalignment when bringing the fiber into contact. Typically, only one edge or protruding part of the fiber tip will touch, allowing for some bending motion that still allows for resonance tuning, while differential motion is strongly suppressed. Figure 4(c) shows the cumulative cavity length jitter for such a situation with active stabilization (green) in comparison with measurements taken without contact.

To illustrate the high mechanical stability when the fiber mirror is in contact, we perform spectroscopy of the cavity resonance, which corresponds to the 11th longitudinal mode order at 580 nm. While the cavity resides on the resonance without active feedback,

we scan the spectroscopy laser (DL pro, TOPTICA GmbH) over the full cavity linewidth at a slow rate of 0.5 Hz to be susceptible to all noise frequency components. The average of ten scans of the cavity transmission signal is plotted in Fig. 4(d) together with a fit of a Lorentzian line. The good overlap with the Lorentzian line confirms the high mechanical stability, leading to a finesse-limited cavity performance over a timespan sufficient for most quantum optics experiments.

B. Cavity stability in a closed-cycle cryostat

We perform analogous measurements for the cavity setup in the closed-cycle cryostat. The transfer function [Fig. 5(a)] does not show any resonances below 4 kHz, which is in accordance with the measurements on the flow cryostat setup and verifies the reproducibility of the design. The highest eigenfrequencies appear around 20 kHz.

The ASD spectra of our best performing configurations with the cavity mirrors in mechanical contact and with optimized clamping of cables and the loose part of the fiber, pre-stress on screws, electric filtering, etc., are shown in Fig. 5(b). Both the passive (blue) and actively stabilized (orange) configuration show a significant improvement in noise compared to the actively stabilized operation without mechanical contact of the mirrors (green).

Similarly to the flow cryostat setup, the fast PID output is low-pass filtered at 1 kHz, and the low noise level above 1 kHz shows the high passive stability of the system. We observe an increase in noise around 1 kHz depending on the PID gain, which is due to

the servo bump of the feedback loop and limits the gain of the fast PID.

In the cumulative depiction, see Fig. 5(c), three main frequencies stand out: the largest fraction of noise in the passive mode at 62 Hz stems from the compressor that pumps the helium into the cold head, the servo bump at 1.058 kHz, and a third contribution at 4.27 kHz, which we attribute to the dominant resonance of the lever arm. Their origins are determined by comparing different experimental settings. Note that the servo bump is absent in the passive configuration. The biggest improvement of the stabilization is a significant decrease in noise introduced by the compressor, showing an almost ten-fold lower rms noise up to that frequency. By integrating over the whole frequency range, we extract a passive stability over the whole cryostat cycle of 2.4 pm rms, which improves to 1.2 pm rms when actively stabilized. In contrast, we obtain 15 pm rms without contact, which is not affected by the active stabilization due to dominating high frequency noise components.

By synchronizing the measurement to the trigger output of the cryostat, we can examine the cavity noise as it is temporally resolved throughout the cold-head cycle. When considering only the quiet phase of the cycle, which spans over several 100 ms and is, therefore, long enough for most spectroscopy experiments, the measurement reveals a cavity length jitter as low as 0.8 pm rms, as shown in Fig. 5(d), corresponding to a noise of <1 % of the cavity linewidth at a finesse of 3700 as used for the stabilization. The cavity parameters of both setups are summarized in Table I. The finesse of our cavities is measured by scanning the cavity length over several free spectral ranges (FSRs) using the coarse piezo and recording the cavity
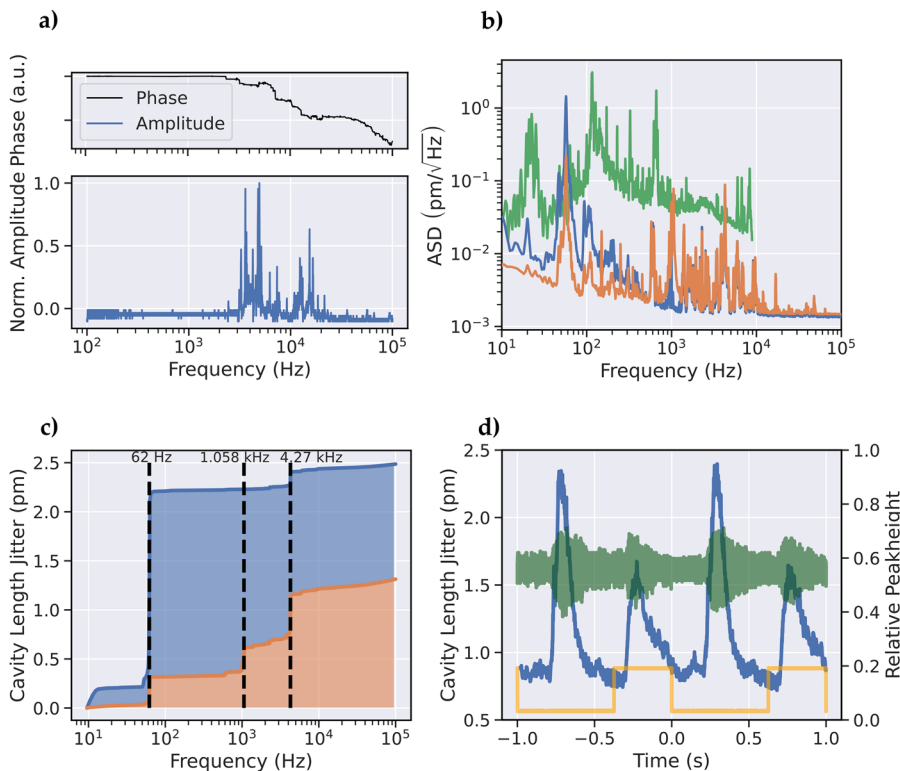

FIG. 5. Cavity stability at 10 K in the closed-cycle cryostat. (a) Mechanical transfer function of the cavity (blue) and its phase response (black). (b) ASD of cavity length fluctuations without (blue, 2.4 pm rms), with active stabilization (red, 1.2 pm rms), and without contact of the fiber and plane mirror (green, 15 pm rms). (c) Cumulative cavity length noise for the respective measurements in (b). (d) Time-resolved cavity noise over two cold head cycles. Yellow: trigger output of the cryostat. The cavity transmission (green) is shown together with the cavity length fluctuation (blue).

TABLE I. Summary of the cavity parameters for the platform installed in a flow cryostat and a closed-cycle cryostat.

Parameter	Flow cryostat	Closed-cycle cryostat
Lock wavelength	640 nm	690 nm
Lock-finesse	1200	3700
Lock-FWHM	260 pm	90 pm
Max. finesse	18 000	37 000
FWHM	15 pm	8.6 pm
$\Delta z_{open,passive}(10\,K)$	5 pm	15 pm
$\Delta z_{open,active}(10\,K)$	2.5 pm	15 pm
$\Delta z_{contact,passive}(10\,K)$	0.8 pm	2.4 pm
$\Delta z_{contact,active}(10\,K)$	0.7 pm	1.2 pm (0.8 pm)

transmission. By fitting a Lorentzian to the resonances, we obtain their temporal width and distance (FSR) to calculate the finesse as the ratio between FSR and width. We use grating stabilized diode lasers (DL pro, TOPTICA GmbH) with a linewidth of about 1 MHz to perform the measurements shown here.

IV. CONCLUSION

In this work, we presented a home-built open-access fiber-based Fabry–Pérot microcavity platform that achieves the highest mechanical stability of better than 1 pm, both in a closed-cycle cryostat and in a flow cryostat. The basis, therefore, is a mechanical design of high intrinsic stiffness, the incorporation of active feedback stabilization, and by bringing the fiber into mechanical contact with the planar mirror. We have demonstrated the reproducibility of our design principles by successfully operating two cavity stages inside two different cryostat types.

The passive stability of a few pm of both setups is already good enough to resign from active stabilization, which requires a second locking laser and a double-resonance condition with the spectroscopy laser. The vibration broadening of the cavity linewidth for a finesse of 20 000 would only reduce the Purcell factor by less than 5% when both mirrors are in contact, and about 10% without mechanical contact in the flow cryostat, respectively (see Fig. 1).

Both designs combine excellent mechanical stability with full three-axis coarse and fine tunability at cryogenic temperatures. Furthermore, the cavity stage facilitates the fast exchange of the planar mirror carrying the sample under investigation. Therefore, this platform is particularly useful for the investigation of many different, spatially and spectrally inhomogeneous samples, where lateral scanning is needed to find suitable emitters and longitudinal tuning is required to target the desired transition. This holds great prospects to enable fundamental studies in the field of solid-state quantum optics and advanced applications in quantum technologies.

ACKNOWLEDGMENTS

AUTHOR DECLARATIONS

Conflict of Interest

The authors have no conflicts to disclose.

Author Contributions

Maximilian Pallmann and Timon Eichhorn contributed equally to this paper.

Maximilian Pallmann: Conceptualization (equal); Data curation (lead); Formal analysis (lead); Investigation (lead); Methodology (lead); Software (lead); Validation (lead); Visualization (lead); Writing – original draft (lead); Writing – review & editing (equal). **Timon Eichhorn**: Conceptualization (equal); Data curation (lead); Formal analysis (lead); Investigation (lead); Methodology (lead); Software (lead); Validation (lead); Visualization (lead); Writing – original draft (lead); Writing – review & editing (equal). **Julia Benedikter**: Conceptualization (equal); Methodology (equal); Software (equal); Writing – review & editing (supporting). **Bernardo Casabone**: Conceptualization (supporting); Methodology (equal); Writing – review & editing (supporting). **Thomas Hümmer**: Conceptualization (supporting); Methodology (equal); Software (lead); Writing – review & editing (supporting). **David Hunger**: Conceptualization (lead); Funding acquisition (lead); Methodology (equal); Project administration (lead); Resources (lead); Supervision (lead); Validation (supporting); Writing – review & editing (equal).

DATA AVAILABILITY

The data that support the findings of this study are available from the corresponding author upon reasonable request.

REFERENCES

[1]N. Tomm, A. Javadi, N. O. Antoniadis, D. Najer, M. C. Löbl, A. R. Korsch, R. Schott, S. R. Valentin, A. D. Wieck, A. Ludwig, and R. J. Warburton, "A bright and fast source of coherent single photons," Nat. Nanotechnol. **16**, 399–403 (2021).

[2]S. Johnson, P. R. Dolan, and J. M. Smith, "Diamond photonics for distributed quantum networks," Prog. Quantum Electron. **55**, 129–165 (2017).

[3]M. Salz, Y. Herrmann, A. Nadarajah, A. Stahl, M. Hettrich, A. Stacey, S. Prawer, D. Hunger, and F. Schmidt-Kaler, "Cryogenic platform for coupling color centers in diamond membranes to a fiber-based microcavity," Appl. Phys. B **126**, 131 (2020).

[4]S. Häußler, G. Bayer, R. Waltrich, N. Mendelson, C. Li, D. Hunger, I. Aharonovich, and A. Kubanek, "Tunable fiber-cavity enhanced photon emission from defect centers in hBN," Adv. Opt. Mater. **9**, 2002218 (2021).

[5] T. Vogl, R. Lecamwasam, B. C. Buchler, Y. Lu, and P. K. Lam, "Compact cavity-enhanced single-photon generation with hexagonal boron nitride," ACS Photonics **6**, 1955–1962 (2019).

[6] J. Benedikter, H. Kaupp, T. Hümmer, Y. Liang, A. Bommer, C. Becher, A. Krueger, J. M. Smith, T. W. Hänsch, and D. Hunger, "Cavity-enhanced single-photon source based on the silicon-vacancy center in diamond," Phys. Rev. Appl. **7**, 024031 (2017).

[7] R. Albrecht, A. Bommer, C. Deutsch, J. Reichel, and C. Becher, "Coupling of a single NV-center in diamond to a fiber-based microcavity," Phys. Rev. Lett. **110**, 243602 (2013).

[8] E. Janitz, M. Ruf, M. Dimock, A. Bourassa, J. Sankey, and L. Childress, "Fabry-Perot microcavity for diamond-based photonics," Phys. Rev. A **92**, 043844 (2015).

[9] D. Riedel, I. Söllner, B. J. Shields, S. Starosielec, P. Appel, E. Neu, P. Maletinsky, and R. J. Warburton, "Deterministic enhancement of coherent photon generation from a nitrogen-vacancy center in ultrapure diamond," Phys. Rev. X **7**, 031040 (2017).

[10] M. Ruf, M. Weaver, S. van Dam, and R. Hanson, "Resonant excitation and Purcell enhancement of coherent nitrogen-vacancy centers coupled to a Fabry-Perot microcavity," Phys. Rev. Appl. **15**, 024049 (2021).

[11] D. Najer, I. Söllner, P. Sekatski, V. Dolique, M. C. Löbl, D. Riedel, R. Schott, S. Starosielec, S. R. Valentin, A. D. Wieck, N. Sangouard, A. Ludwig, and R. J. Warburton, "A gated quantum dot strongly coupled to an optical microcavity," Nature **575**(7784), 622–627 (2019).

[12] D. Wang, H. Kelkar, D. Martin-Cano, D. Rattenbacher, A. Shkarin, T. Utikal, S. Götzinger, and V. Sandoghdar, "Turning a molecule into a coherent two-level quantum system," Nat. Phys. **15**, 483–489 (2019).

[13] F. Li, Y. Li, Y. Cai, P. Li, H. Tang, and Y. Zhang, "Tunable open-access microcavities for solid-state quantum photonics and polaritonics," Adv. Quantum Technol. **2**, 1900060 (2019).

[14] S. Dufferwiel, S. Schwarz, F. Withers, A. A. P. Trichet, F. Li, M. Sich, O. Del Pozo-Zamudio, C. Clark, A. Nalitov, D. D. Solnyshkov, G. Malpuech, K. S. Novoselov, J. M. Smith, M. S. Skolnick, D. N. Krizhanovskii, and A. I. Tartakovskii, "Exciton-polaritons in van der Waals heterostructures embedded in tunable microcavities," Nat. Commun. **6**, 8579 (2015).

[15] L. C. Flatten, Z. He, D. M. Coles, A. A. P. Trichet, A. W. Powell, R. A. Taylor, J. H. Warner, and J. M. Smith, "Room-temperature exciton-polaritons with two-dimensional WS$_2$," Sci. Rep. **6**, 33134 (2016).

[16] C. Gebhardt, M. Förg, H. Yamaguchi, I. Bilgin, A. D. Mohite, C. Gies, M. Florian, M. Hartmann, T. W. Hänsch, A. Högele, and D. Hunger, "Polariton hyperspectral imaging of two-dimensional semiconductor crystals," Sci. Rep. **9**, 13756 (2019).

[17] M. Aspelmeyer, T. J. Kippenberg, and F. Marquardt, "Cavity optomechanics," Rev. Mod. Phys. **86**, 1391–1452 (2014).

[18] A. D. Kashkanova, A. B. Shkarin, C. D. Brown, N. E. Flowers-Jacobs, L. L. Childress, S. W. Hoch, L. Hohmann, K. Ott, J. Reichel, and J. G. E. Harris, "Superfluid Brillouin optomechanics," Nat. Phys. **13**, 74 (2016).

[19] F. Rochau, I. Sánchez Arribas, A. Brieussel, S. Stapfner, D. Hunger, and E. M. Weig, "Dynamical backaction in an ultrahigh-finesse fiber-based microcavity," Phys. Rev. Appl. **16**, 014013 (2021).

[20] Y. Fontana, R. Zifkin, E. Janitz, C. D. Rodríguez Rosenblueth, and L. Childress, "A mechanically stable and tunable cryogenic Fabry–Pérot microcavity," Rev. Sci. Instrum. **92**, 053906 (2021).

[21] B. Casabone, C. Deshmukh, S. Liu, D. Serrano, A. Ferrier, T. Hümmer, P. Goldner, D. Hunger, and H. de Riedmatten, "Dynamic control of Purcell enhanced emission of erbium ions in nanoparticles," Nat. Commun. **12**, 3570 (2021).

[22] S. Vadia, J. Scherzer, H. Thierschmann, C. Schäfermeier, C. Dal Savio, T. Taniguchi, K. Watanabe, D. Hunger, K. Karraï, and A. Högele, "Open-cavity in closed-cycle cryostat as a quantum optics platform," PRX Quantum **2**, 040318 (2021).

[23] T. Ruelle, D. Jaeger, F. Fogliano, F. Braakman, and M. Poggio, "A tunable fiber Fabry–Perot cavity for hybrid optomechanics stabilized at 4 K," Rev. Sci. Instrum. **93**, 095003 (2022).

[24] B. Merkel, A. Ulanowski, and A. Reiserer, "Coherent and Purcell-enhanced emission from erbium dopants in a cryogenic high-Q resonator," Phys. Rev. X **10**, 041025 (2020).

[25] D. Hunger, T. Steinmetz, Y. Colombe, C. Deutsch, T. W. Hänsch, and J. Reichel, "A fiber Fabry–Perot cavity with high finesse," New J. Phys. **12**, 065038 (2010).

[26] J. F. S. Brachmann, H. Kaupp, T. W. Hänsch, and D. Hunger, "Photothermal effects in ultra-precisely stabilized tunable microcavities," Opt. Express **24**, 21205–21215 (2016).